STM JOURNALS

International Journal of
Membranes

Volume 1, Issue 1, 2024
January—June
DOI (Journal): 10.37591/IJM

https://journals.stmjournals.com/ijm

Research IJM

Optimization of Gas Sensitivity of CuO/Carbon Composites with Carbon Particles Synthesized from Acacia Auriculiformis Branches

C. A. Samarahewa[1], Sunil Dehipawala[2], P. Samarasekara[3,*]

Abstract

Carbon particles fabricated from the core of acacia tree branches were utilized to synthesize CuO/carbon composite films. The gas sensing properties of these films grown on glass substrates using the doctor blade method were measured in 1000 ppm of methanol vapor at the room temperature. All the films were annealed at 75 ^{0}C for 1 hour in air. The structure, the optical band gap and the surface morphology of the samples were determined using XRD patterns, UV-Visible spectrums and SEM micrographs, respectively. The XRD findings suggested that a single phase of CuO might crystallise as thin films. The XRD patterns were used to assess the samples' average crystallite size, strain, and dislocation density. The peaks of carbon were not visible in the XRD patterns of the films with CuO/carbon due to the amorphous nature of carbon. Platelet particles were observed in SEM images of pure carbon samples. Mass ratio between cupric oxide (CuO) and carbon particles was varied to optimize the gas sensitivity. The gas sensitivity of carbon could be enhanced by adding CuO powder. The highest gas sensitivity (1.43) was measured for the film with 90% CuO and 10% carbon particles.

Keywords: Cupric oxide, carbon, acacia, gas sensitivity, methanol vapor

INTRODUCTION

Both metal oxides and carbon based materials are prime candidates of gas sensors. Carbon powders can be found in different forms such as activated carbon and organic carbon. Activated carbon has a considerably larger band gap than organic carbon. The band gap of activated carbon is in the range of 2.80 to 3.15 eV. The band gap of organic carbon powders is in the range of 1.7 to 1.8 eV. Carbon powders find potential applications in removal of pollutants, water treatment, air purification, precious metal recovery and gas sensors. Carbon powders have been synthesized from different types of woods or biomass such as oil palm shells, date pits, pinewood, mahogany, eucalyptus, chestnut, cedar, walnut, oak, rubber, fir, teak, cedar and acacia. In various production methods, different acids are used to activate carbon.

*Author for Correspondence
P. Samarasekara
E-mail: pubudus@pdn.ac.lk

[1]Research assistant, Department of Physics, University of Peradeniya, Peradeniya, Sri Lanka
[2]Associate Professor, Physics Department, Queensborough Community College of CUNY, Bayside, NY 11364, USA
[3]Senior Professor, Department of Physics, University of Peradeniya, Peradeniya, Sri Lanka

Received Date: April 09, 2024
Accepted Date: May 15, 2024
Published Date: May 21, 2024

Citation: C. A. Samarahewa, Sunil Dehipawala, P. Samarasekara. Optimization of Gas Sensitivity of CuO/Carbon Composites with Carbon Particles Synthesized from Acacia Auriculiformis Branches. International Journal of Membranes. 2024; 1(1): 22–30.

Activated carbon has been prepared from pine wood under conditions with carbonization rate of 550 ^{0}C/4h and activation rate of 900 ^{0}C/0.5-4h [1]. Activated carbon has been synthesized from chestnut wood under conditions with carbonization rate of 450^{0}C/4h and chemical treatment of H_3PO_4 [2]. Activated carbon has been fabricated from fir wood under conditions with carbonization rate of 450^{0}C/1.5h, activation rate of 780 ^{0}C/1h and chemical treatment of KOH [3]. Mahogany

sawdust has been employed to prepare activated carbon with adsorbate of direct blue 2B and adsorption capacity 518 mg/g [4]. Eucalyptus wood has been employed to prepare activated carbon with adsorbate of phenol [5]. Fir wood has been employed to prepare activated carbon with adsorbate of basic brown 1 and adsorption capacity 1476.3 mg/g [6].

This is an overview of the research on metal oxide and carbon-based gas sensors. The functionality of side walls of carbon nanotubes is crucial in enhancement of the gas sensitivity and the selectivity [7]. Carbon based materials such as graphene has less crystal defects, higher electrical conductivity and less noise levels [8]. Doping B and N improves the conductivity of carbon nanotubes are able to detect hazardous gases due to pyridine type sites [9]. Multi-walled carbon nanotubes synthesized using a chemical vapor deposition method has been employed to detect hydrogen and methane gases. The electrical resistivity of carbon nanotube samples decreases and increases in H_2 and CH_4 gases, respectively, due to the oxidation and reduction processes [10]. Tungsten oxide films prepared from vacuum evaporation has been used to detect methane and nitric oxide gases. The gas sensitivity of tungsten oxide films with different thicknesses have been measured in different operating temperatures. Thicker tungsten oxide films have provided higher gas sensitivities [11]. The highest gas sensitivity of ferric oxide thin films was measured at the operating temperature of 170 ^{0}C for CO_2 gas [12].

In this manuscript, the enhancement of gas sensitivity of carbon added CuO films measured in 1000 ppm of methanol vapor at the room temperature will be described. The organic carbon powders were prepared from the core of acacia tree branches available in Sri Lanka.

EXPERIMENTAL

A mixture of PEG binder and carbon/CuO was employed to fabricate films [12, 13]. Carbon powder was extracted from the core of acacia auriculiformis tree branches using the technique described by Saleem et al [14]. The amount of carbon powder in CuO:Carbon mixture was varied from 5 to 100%.

The structure, optical band gap and the morphology of films were determined by means of a Rigaku Ultima IV X-ray diffractometer, a Shimadzu 1800 UV-Vis spectrophotometer and a Zeiss EVO LS15 Scanning electron microscope (SEM), respectively. Electric current passes only through the sample since the central portion of the conductive layer was removed. The resistance of the sample was taken into consideration when choosing the value of the standard resistor. Gold coated Cu wires were used to reduce the contact resistances.

RESULTS AND DISCUSSION

Figure 1 delineates the X-ray Diffraction (XRD) patterns of films of CuO/carbon mixtures. All the peaks belong to the phase of pure CuO. The XRD pattern of the sample with 10%CuO is similar to the XRD patterns of the samples with 90%CuO and 95%CuO. Figure 2 shows the XRD pattern of pure carbon sample synthesized from the core of acacia tree branches. The broad peaks indicate the amorphous properties of carbon sample [15, 16]. In the XRD patterns of samples with CuO, peaks of carbon are not visible due to the amorphous nature of carbon. Only the peaks of highly crystallized CuO are visible in the Figure 1. When the carbon atoms fill the vacant sites of CuO lattice, the crystal structure of CuO does not change. The sample's XRD pattern remains unchanged as a result of the carbon atoms' addition. On the other hand, if the carbon particles are trapped inside the CuO particles, XRD detects only the CuO atoms.

Crystallite size (D), dislocation density (δ) and strain (ε) of the samples were calculated using $D = \frac{0.91\lambda}{\beta \cos\theta}$, $\delta = \frac{1}{D^2}$ and $\varepsilon = \frac{\beta \cos\theta}{4}$, respectively. λ and β are 1.54060 ^{0}A and the full width at half

maximum (FWHM) of XRD peak at angle θ, respectively [13]. (002) and (111) peaks of the XRD patterns given in Figure 1 and (002) peak given in Figure 2 were used for these calculations. The calculated values of crystallites sizes, strains and dislocation densities are given in Table 1.

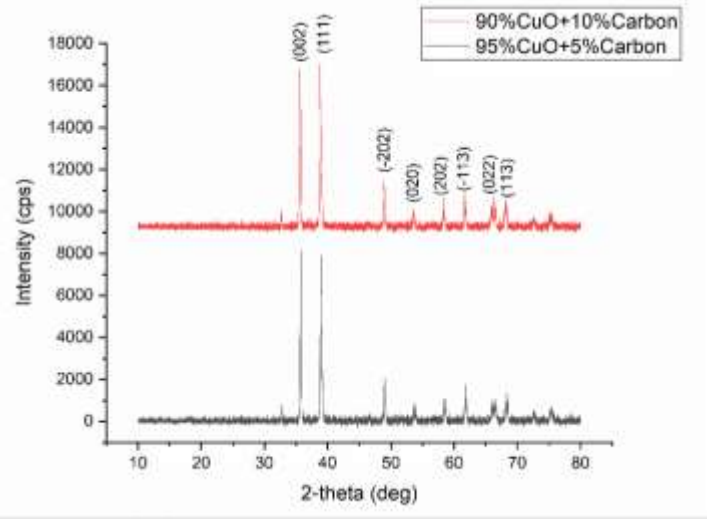

Figure 1. XRD patterns of samples with 90%CuO and 95%CuO.

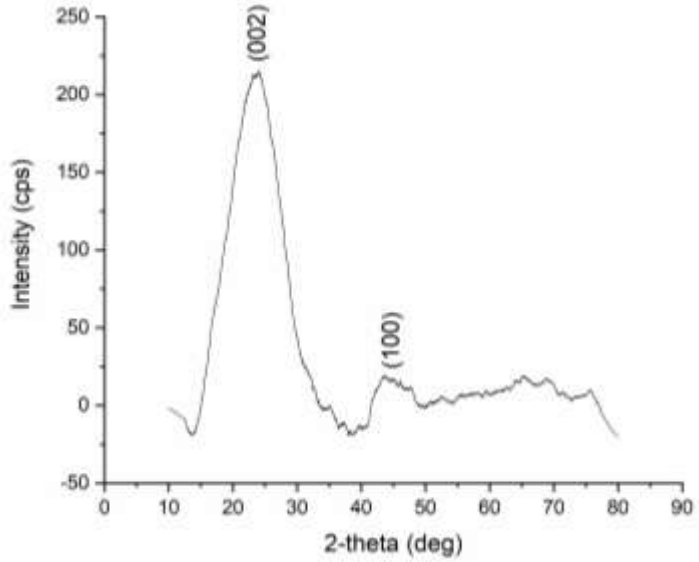

Figure 2. XRD pattern of pure carbon sample synthesized from the acacia tree branches.

Table 1. Values of average crystallite size, dislocation density and strain of samples.

Sample	Angle 2θ(deg)	Angle θ (deg)	FWHM (deg)	FWHM (rad)	Crystallite size (nm)	Dislocation density (10^{14} lines/m^2)	Strain
Pure carbon	24.08	12.04	9.09	0.15871	0.903	12258.40	0.03881
95%CuO	35.78	17.89	0.17	0.00297	49.633	4.06	0.00071
90%CuO	38.85	19.43	0.21	0.00367	40.545	6.08	0.00086

The addition of CuO particles has significantly increased the average crystallite size of samples. This implies that the average crystallite size of carbon particles is much smaller than those of CuO. As a result, the strain and the dislocation density of pure carbon sample are much larger than those of CuO added samples. The amorphous nature of the pure carbon sample is responsible for the higher dislocation density and strain. This data implies that the average particle size of pure carbon is much smaller than that of CuO.

Figure 3 delineates three UV-Visible spectrums of pure carbon, samples with 90%CuO and 95% CuO. Tangential lines were drawn at the points of absorption curve with the highest slop to find the absorption edges. However, the point with zero absorption is not marked on the vertical axis of the spectrum in order to show the shape of the spectrum clearly. The absorption edges of the pure carbon sample were observed at 234.9 and 324.2 nm. The absorption edges of the samples with 90%CuO and 95%CuO were found to be 548.1 and 507.8 nm, respectively. The optical band gaps of the samples with 90%CuO and 95%CuO are 2.26 and 2.44 eV, respectively. Two different optical band gaps were observed in pure carbon such as 5.28 and 3.28 eV. According to some previous studies, energy gap of pure carbon is about 5.4 eV. Therefore, the band gap at 5.28 eV corresponds to pure carbon. Band gaps of many metal oxides such as TiO_2, NiO, SnO_2 and metal alloys possess band gap closer to 3.76 eV. Therefore, the band gap at 3.28 eV may be related to the existence of a trace of amount of metal oxide or alloy in the carbon sample. If the quantity of this impurity is infinitesimal, then it will not be detected in the XRD pattern.

Although the band gap of pure CuO is in the range from 1.2 to 1.9 eV, the band gap of our CuO samples mixed with carbon is higher than 1.9 eV because the band gap of pure carbon is much higher than the band gap of pure CuO. Addition of CuO has decreased the band gap of carbon due to the addition of extra energy levels. At higher CuO concentrations, the field inside crystal fluctuates due to due to the scattering of conduction electrons. As a result, adding more CuO (95%CuO) has slightly increased the band gap. Because the band gap of CuO is much less than that of carbon, all the electrons jump from the valence band to conduction band when the energy of photon is equal to the band gap of CuO. Therefore, the band gap of carbon is not visible in the UV-visible spectrum of films with a mixture of CuO and carbon.

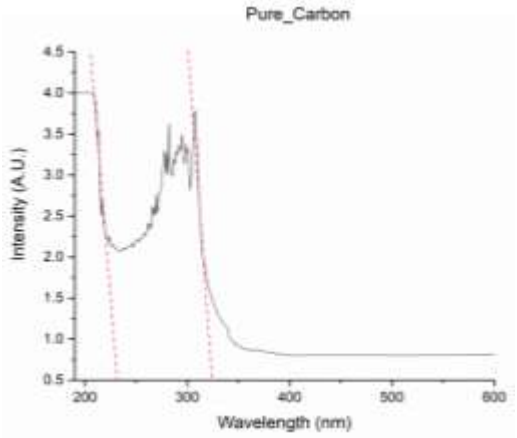

(a) Pure Carbon

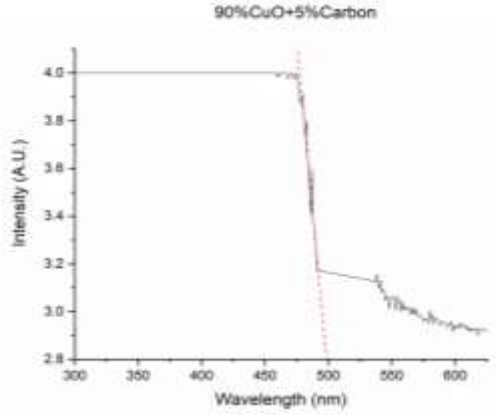

(b) 90%CuO

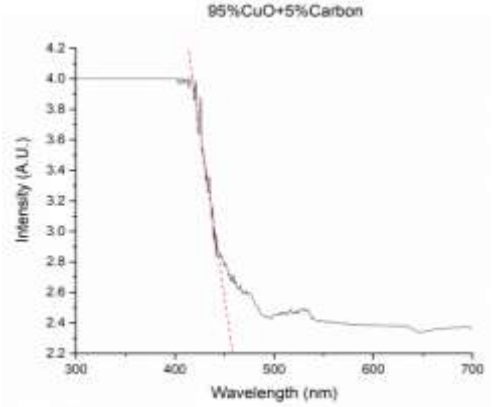

(c) 95%CuO

Figure 3. UV-visible spectrums of pure carbon(a), 90%CuO (b)and 95%CuO samples (c).

Figure 4 represents the graphs of the voltage (*V*) measured across the standard resistor versus time for each sample at the room temperature. After introducing 1000 ppm of methanol vapor to the sample, the voltage increased. After removing the methanol vapor, the voltage decreased. The amount of change of the voltage is different for different samples. The graphs of the electric current versus time for each sample at the room temperature are shown in Figure 5. The resistance of the sample (*R*) is given by

$$5 = V+IR \rightarrow \quad (1)$$

The graphs of the resistance of each sample versus time at the room temperature are shown in Figure 6.

The gas sensitivity (*S*) of the samples was calculated from [12, 13]

$$S = \frac{R_i - R_f}{R_f} \quad (2)$$

The gas sensitivity, response time and recovery time of each sample calculated from the values given in Figure 6 are tabulated in Table 2. The response time of samples significantly changes with doping concentration. However, the recovery time does not vary significantly. According to our previous studies, the samples with the highest gas sensitivity possess the highest response and recovery times [11]. However, the samples given in Table 2 behave in the opposite manner.

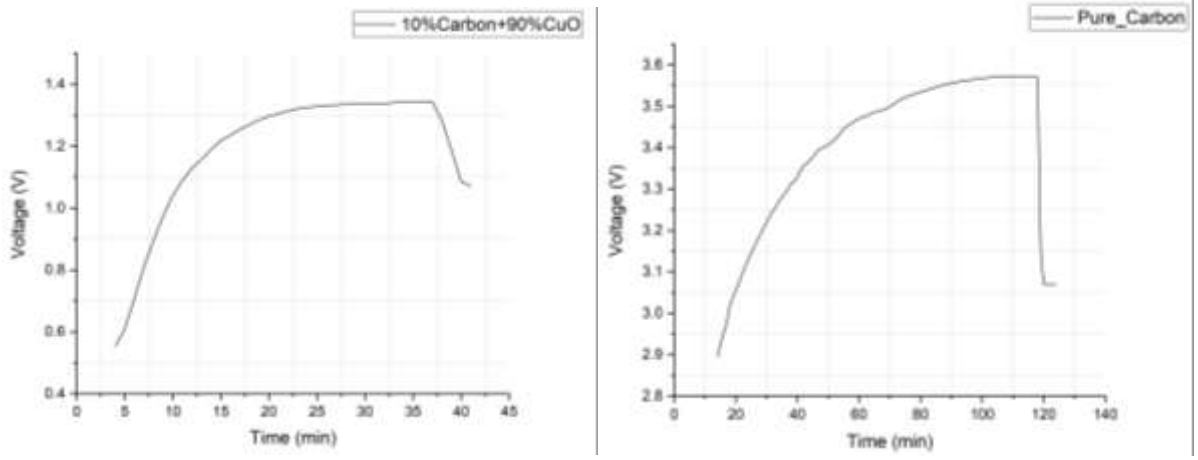

(a) (b)

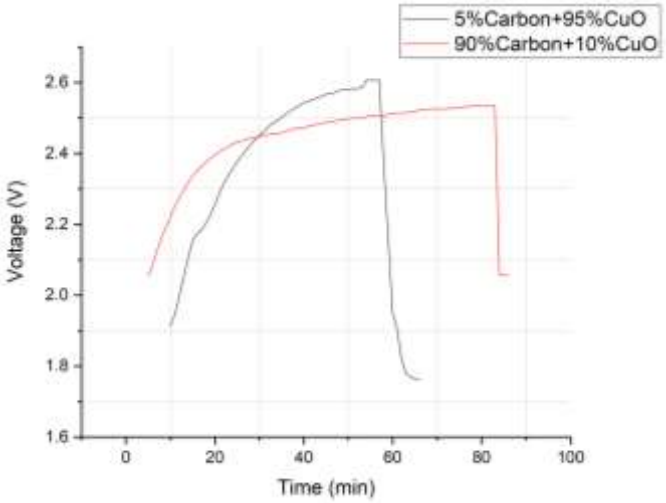

(c)

Figure 4. Voltage versus time graphs of composites with different CuO and carbon ratios measured in 1000 ppm of methanol.

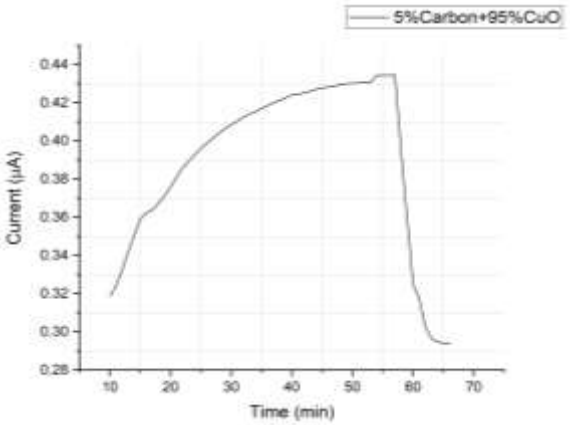

(a)

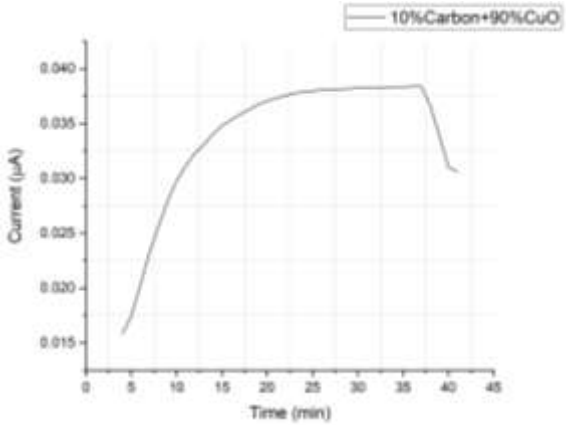

(b)

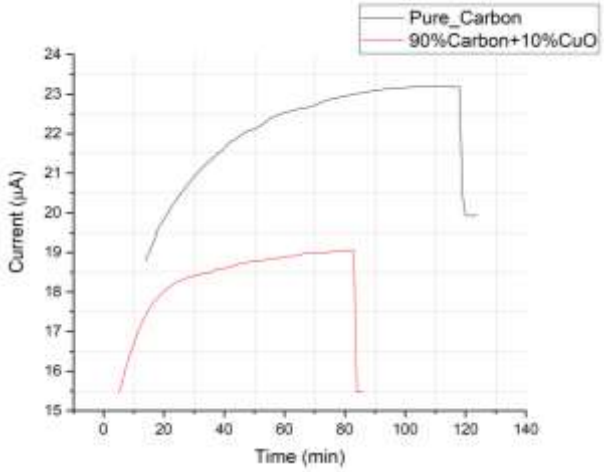

(c)

Figure 5. Current versus time graphs of composites with different CuO and carbon ratios measured in 1000 ppm of methanol.

Table 2. Gas sensing properties of films with different CuO:carbon ratios.

Sample	Gas sensitivity	Response time (min)	Recovery time (min)
Pure Carbon	0.82	90	4
10%CuO	1.00	74	2
90%CuO	2.64	32	3
95%CuO	1.88	44	7

The oxygen ions in CuO are responsible for the change of resistance due to the reduction reaction. On the other hand, oxygen atoms trapped inside carbon structure is responsible for the change in the resistance. The sample with 10% of carbon provides the highest gas sensitivity. The gas sensitivity of all the samples with CuO is higher than that of pure carbon. Because the outer surface is mostly responsible for the adsorption of gas or vapor, it is reasonable to assume that CuO and carbon serve as the outer part and inner part of the particles, respectively, in this composite. The thickness of the CuO layer outside the carbon particle varies with the addition of more CuO particles. At some optimum value of the thickness of CuO layer, the adsorption will be higher. The same effect of ZnO depletion layer on the gas sensitivity of ammonia vapor has been observed [17]. According to the XRD data, the smaller carbon particles can be trapped inside the larger CuO particles. Therefore, the enhancement of the gas sensitivity agrees with data found from the XRD patterns. In addition, the dopant will effect on change in morphology, formation of stoichiometric solid solution, activation energy, generating oxygen vacancy and change in electronic structure. These factors are also attributed to the alteration of the gas sensitivity. Doping makes influence on the carrier mobility and surface states. As a result, the electrical properties of samples alter with the doping concentration.

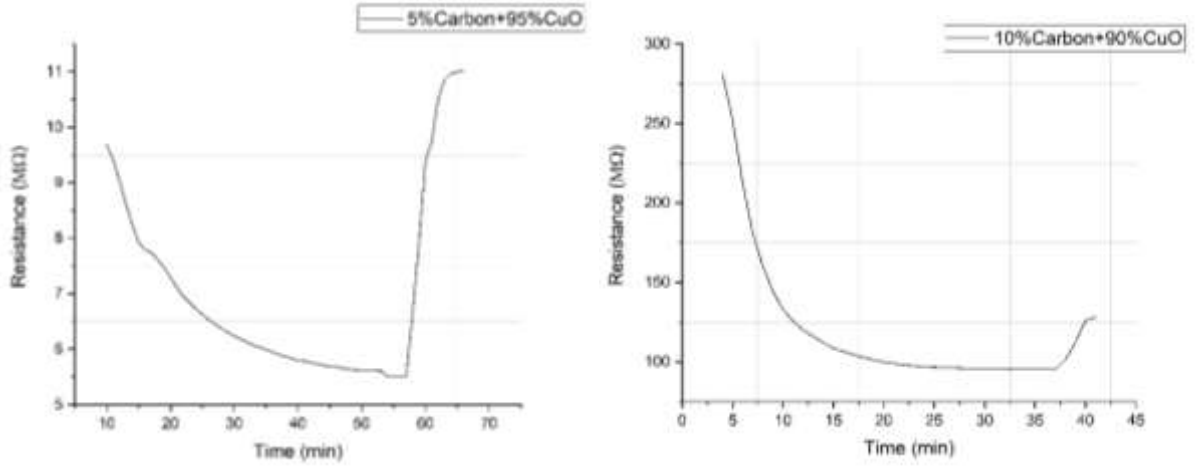

(a) (b)

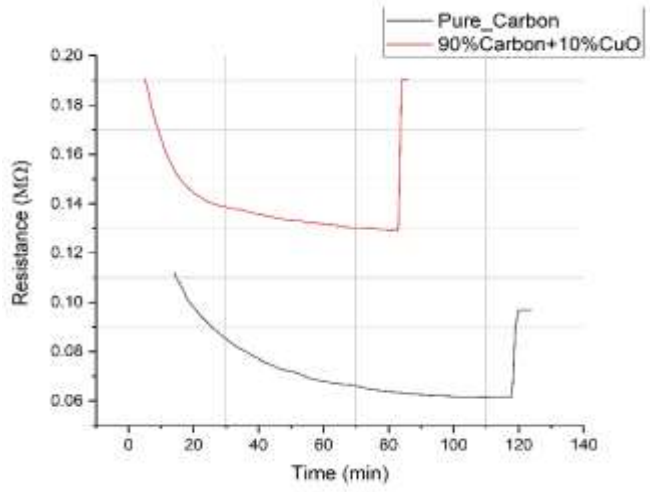

(c)

Figure 6. Resistance versus time graphs of composites with different CuO and carbon ratios measured in 1000 ppm of methanol.

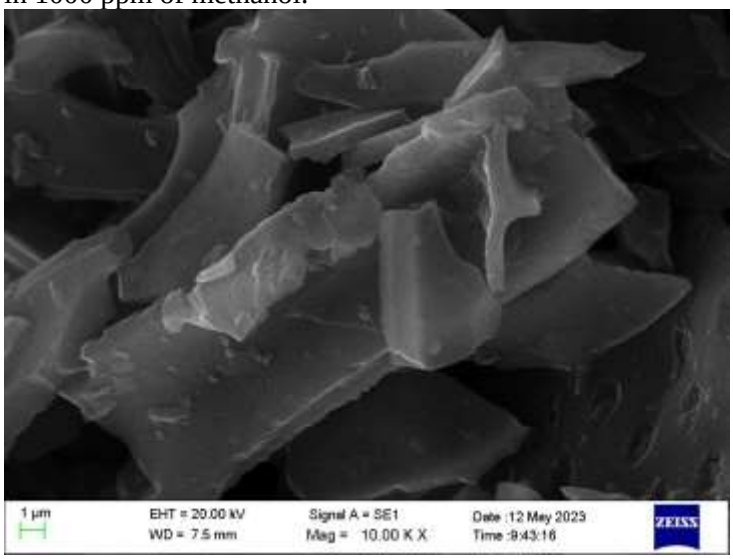

Figure 7. SEM image of carbon film synthesized from acacia.

According to the UV-visible spectrums, the film with 90%CuO possesses the lowest band gap. This lowest band gap is attributed the highest gas sensitivity of the film with 90%CuO.

Figure 7 elaborates the SEM image of pure carbon sample synthesized from carbon powder prepared from the core of acacia tree branches. The sample is consists of platelet particles. The side with larger surface area of the platelet particles is facing the gas or vapor. This nature of particles is helpful to enhance the adsorption of gas or vapor. The size of carbon particles varies in a wide range.

CONCLUSIONS

Because the addition of CuO enhances the gas sensitivity of carbon, it can be concluded that carbon particles are trapped inside CuO particles in the composite. In addition, it is evident that the outer CuO layer of particles in the sample is responsible for the adsorption of vapor. The best gas sensitivity (2.64) and the best response time (32 min) were measured for the sample with 90%CuO and 10% carbon in 1000 ppm at the room temperature. Because low cost conductive glass plates were used as substrates, the response times of our samples were higher. Using expensive gold or silver coating as a catalyst will reduce the response time. The average crystallite size in the samples significantly

increased from 0.903 to 49.633 nm due to the addition of CuO powder. Because samples with higher crystallite size provide the higher gas sensitivity, the particle size is not responsible for the higher gas sensitivity of sample with 90%CuO. The strain and the dislocation density of the pure carbon sample were higher than those of the samples with CuO due to the amorphous nature of the samples. Furthermore, the lowest band gap the film with 90%CuO is attributed the highest gas sensitivity.

REFERENCES

1. Tseng RL, Wu FC, Juang RS. Liquid-phase adsorption of dyes and phenols using pinewood-based activated carbons. Carbon. 2003 Jan 1;41(3):487-95.
2. Dıaz-Dıez MA, Gómez-Serrano V, González CF, Cuerda-Correa EM, Macıas-Garcıa A. Porous texture of activated carbons prepared by phosphoric acid activation of woods. Applied surface science. 2004 Nov 15;238(1-4):309-13.
3. Wu FC, Tseng RL, Juang RS. Preparation of highly microporous carbons from fir wood by KOH activation for adsorption of dyes and phenols from water. Separation and purification technology. 2005 Dec 1;47(1-2):10-9.
4. Malik PK. Dye removal from wastewater using activated carbon developed from sawdust: adsorption equilibrium and kinetics. Journal of Hazardous Materials. 2004 Sep 10;113(1-3):81-8.
5. Tancredi N, Medero N, Möller F, Píriz J, Plada C, Cordero T. Phenol adsorption onto powdered and granular activated carbon, prepared from Eucalyptus wood. Journal of colloid and interface science. 2004 Nov 15;279(2):357-63.
6. Wu FC, Tseng RL. Preparation of highly porous carbon from fir wood by KOH etching and CO2 gasification for adsorption of dyes and phenols from water. Journal of Colloid and Interface Science. 2006 Feb 1;294(1):21-30.
7. Peng S, Cho K. Ab initio study of doped carbon nanotube sensors. Nano letters. 2003 Apr 9;3(4):513-7.
8. Novoselov KS, Geim AK, Morozov SV, Jiang D, Katsnelson MI, Grigorieva IV, Dubonos S, Firsov AA. Two-dimensional gas of massless Dirac fermions in graphene. nature. 2005 Nov 10;438(7065):197-200.
9. Hsu WK, Firth S, Redlich P, Terrones M, Terrones H, Zhu YQ, Grobert N, Schilder A, Clark RJ, Kroto HW, Walton DR. Boron-doping effects in carbon nanotubes. Journal of Materials Chemistry. 2000;10(6):1425-9.
10. Samarasekara P. Hydrogen and methane gas sensors synthesis of multi-walled carbon nanotubes. Chinese Journal of Physics. 2009 Jun 1;47(3):361-9.
11. Samarasekara P. Gas sensing properties of tungsten oxide thin films in methane and nitric oxide gases. Nitric Oxide. 2009;2:44-50.
12. Samarasekara P, Gunasinghe MS, Karunarathna PG, Madusanka HT, Fernando CA. Temperature dependence of gas sensitivity of ferric oxide thin films in CO2 gas, acetone, ethanol and methanol vapors. GESJ: Physics. 2019;2(22):3-11.
13. Rajapaksha RMTD, Samarasekara P, Karunarathna PGDCK, Bandara TMWJ, Fernando CAN. Enhancement of gas sensitivity of ferric oxide thin films by adding activated carbon nanoparticles. Ionic research and engineering journals (IRE) 2021; 4(10): 107-13.
14. Saleem M, Ali M, Siddiqi Z, Qahtani ASA. Preparation of activated carbon from acacia (Vachelliya seyal) tree branches and application to treat wastewater containing methylene blue dye. Modern. Appl. Sci. 2017; 11(12): 102-8.
15. Farma R, Wahyuni F, Awitdrus A, Deraman MB. Physical properties analysis of activated carbon from oil parm empty fruit bunch fiber on methylene blue absorption. J. Technomaterial Phys. 2019; 1(1): 69-75.
16. Girgis BS, Temerk Y, Gadelrab MM, Abdullah ID. X-ray diffraction patterns of activated carbon prepared under various conditions. Carbon Letters 2007; 8(2): 95-100.
17. Mani GK, Rayappan JBB. A highly selective and wide range ammonia sensor—nanostructured ZnO: Co thin film. Mater. Sci. Eng., B 2015; 191: 41–50.

